

Minimizing the angular divergence of high-order harmonics by truncating the truncated Bessel beam

Peng Ye, Hao Teng,* Xin-Kui He, Shi-Yang Zhong, Li-Feng Wang, Min-Jie Zhan, Wei Zhang, Chen-Xia Yun, and Zhi-Yi Wei†
Beijing National Laboratory for Condensed Matter Physics, Institute of Physics, Chinese Academy of Sciences, Beijing 100190, China

(Received 10 August 2014; published 5 December 2014)

We have experimentally investigated high-order-harmonic generation driven by a few-cycle truncated Bessel (TB) laser beam which propagates through optical elements of finite aperture sizes. The TB beam was first investigated by Nisoli *et al.* [*Phys. Rev. Lett.* **88**, 033902 (2002)], who assumed an infinite size for the optical elements so they concluded that the phase and intensity of the laser field oscillate dramatically around the laser focus in space. However, in all real experiments, the optical elements are always finite in size and would further truncate the TB beam, and so the oscillations would dwindle substantially. In this paper we take the finite size of the optical elements into account. We find that the further truncated TB beam has two intensity peaks around the focus. In front of the second peak position the curvatures of the laser phase front and the atomic-dipole phase front have the same absolute values but opposite signs, so the generated harmonic has a flat wavefront and hence a minimized angular divergence. In addition, at this position the pump intensity is not much less than its maximal value. This result is of significant importance in practical applications due to the finite aperture size of all real optical elements.

DOI: [10.1103/PhysRevA.90.063808](https://doi.org/10.1103/PhysRevA.90.063808)

PACS number(s): 42.65.Ky, 42.65.Re, 42.25.Gy

I. INTRODUCTION

Extreme ultraviolet coherence sources based on high-order-harmonic generation (HHG) has promoted the development of many research fields, such as studies on collective electron dynamics [1], coherent diffractive imaging [2], free electron laser seeding [3], attosecond pulse generation [4], and so forth. All these applications require good spatial characteristics of the harmonics, i.e., small angular divergence and energy concentrated in the center. In general, the small divergence is beneficial for laser propagation, and central concentration gives a good focus. These two characteristics usually appear along with each other.

As is well known, HHG is an extremely nonlinear process. When a strong femtosecond laser pulse is focused into some medium such as a noble gas, light is emitted with a photon energy of typically dozens to hundreds times that of the pump laser [5,6]. Optimization of the spatial properties of the harmonics, especially minimization of the angular divergence, has been investigated over the past two decades. One method is to utilize the phase matching effect. When the pump laser delivers a Gaussian beam and the interactive medium is located behind the laser focus, suitable phase matching would wash out the harmonics with large emission angles, so only those with small emitting angles remain [7–9]. However, at this position the pump intensity is much lower than that at the focus point, so the efficiency is relatively low, plus it is a waste of laser energy.

The second method is to reduce the phase change in the radial direction of the harmonic generation. The total phase of the q th order harmonic can be written as [10]

$$\phi_q(r, z) = q\phi_{\text{laser}}(r, z) + \phi_{\text{int}}(r, z), \quad (1)$$

where ϕ_{laser} is the phase of the fundamental laser. ϕ_{int} is the intensity-dependent atomic-dipole phase and can be expressed

as $\phi_{\text{int}} \approx \alpha I_{\text{laser}}$, where α is the coefficient of the intensity-dependent atomic-dipole phase and I_{laser} is the intensity of the pump laser. r and z are the coordinates of the radial and laser propagation directions respectively. Thus the variation of the harmonic phase depends on the variation of the laser phase as well as the laser intensity. By using a flat-top fundamental beam [11,12] and a loose focusing configuration [13] we can both reduce the variations of the intensity and the laser phase in the radial direction and contain the harmonic emission within a small angle. In this method the variation of the two phases in the radial direction is a disadvantage for the generation of high-order harmonics with small angular divergence, so we must try to eliminate the variations.

In this work we do not try to restrict the radial variation of the two phases but utilize this to flatten the total harmonic phase front. Under proper conditions the phase fronts of ϕ_{int} and ϕ_{laser} bend in opposite directions, so the final harmonic phase front becomes flat and the harmonic only diverges slightly in the far field. To achieve this aim a truncated Bessel (TB) beam, which propagates through the optical elements with a finite size, is used. Nisoli *et al.* [14] first analyzed bright collimated high-order harmonic generation driven by a TB beam. They found that the TB beam has a truncated Bessel intensity profile at the output of the hollow fiber and assumed that the optical elements which the TB beam propagates through are infinite in size. The TB beam has two intensity peaks near the laser focus point along the direction of laser propagation. In the middle between these two peaks the phase and amplitude of the light field oscillate fast in space. However, in practical experiments the mirrors and other optical elements such as the hard aperture are always finite in size and would further truncate the TB beam, so the fast oscillations would vanish and the characteristics of the high-order harmonics described in previous works may be rather different [14–16].

In the following, we first compare the spatial distributions of three beams: the TB beam where the optical elements are finite in size and the TB and the Gaussian beams where the optical elements are infinite in size. There are three characteristics of

*hteng@iphy.ac.cn

†zywei@iphy.ac.cn

the TB beam that are beneficial for the generation of high-order harmonics with small angular divergence. The first is that by putting a medium in front of the second peak intensity point a large curvature of the laser phase front may be obtained, which cancels out the curvature of the atomic-dipole phase front in the opposite direction, flattens the harmonic phase front, and minimizes the angular divergence of the emitted harmonic. Second, in this position the light intensity is still quite high. Third, around the beam focus the curvature of the harmonic phase front has several extrema that are good for phase matching. We provide both experimental and numerical results to verify our analysis.

II. SPATIAL DISTRIBUTION OF THE TRUNCATED BESSEL BEAM WITH FINITE APERTURE SIZE

A schematic of the optical path of our experiment is shown in Fig. 1. A laser beam of 25 fs temporal width, 1 mJ energy, and 1 kHz repetition rate is focused into a fused silica hollow fiber of inner diameter of 250 μm [17]. The hollow fiber is differentially pumped [18] with neon gas and emits a TB beam [14], which is then collimated by a spherical mirror of 1 m focal length, compressed temporally by a set of chirped mirrors, truncated by a hard aperture of 8 mm radius, and finally focused by a spherical mirror of 0.5 m focal length into a gas cell to generate high-order harmonics. The radius of all the mirrors is 12.7 mm. The typical parameters of the final pump laser beam are 0.4 mJ and 4–7 fs.

The propagation of the laser beam is assumed to obey the paraxial wave equation or, equivalently, Huygens integral [19]. For an axial-symmetric lenslike system, the Huygens integral can be simplified by the ABCD matrix [15,20]. Based on this method, previous studies [14–16] which neglected the aperture size of the optical elements gave the spatial distribution of the TB beam around the focus point as shown in Fig. 2(a), where we can see that the intensity oscillates dramatically near the laser focus ($z = 0$). Below, we use the fast discrete Fourier transform to calculate the Huygens integral [21]. The spatial distribution of the laser beam at the exit of the hollow fiber can be expressed as $u(r) = E_0 J_0(2.405r/a)$ with $r < a$, where E_0 is the on-axis peak amplitude, $a = 125 \mu\text{m}$ is the inner radius, and J_0 is the zeroth-order Bessel function of the first kind. The light field $u_{s1}(r)$ in front of the collimating mirror is calculated by the Huygens integral, while the field after the collimating

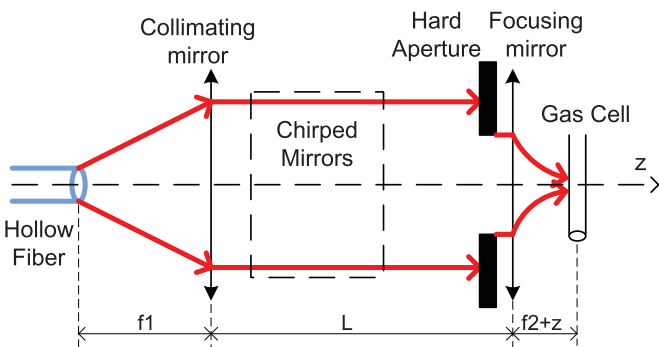


FIG. 1. (Color online) Schematic of optical path in the experimental setup.

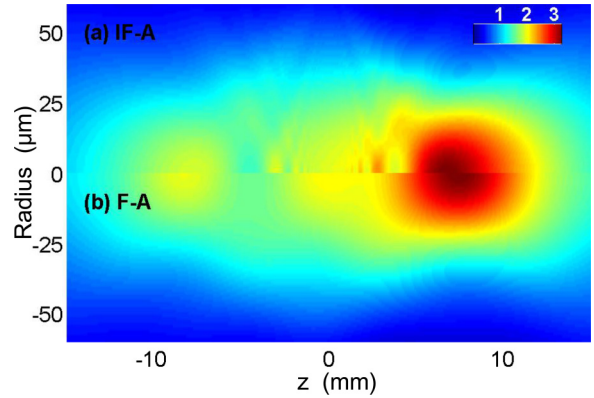


FIG. 2. (Color online) Simulated intensity distributions of the TB beam around the laser focus point for (a) infinite-aperture (IF-A) and (b) finite-aperture (F-A) optics. Both panels use the same linear color bar.

mirror can be expressed as $u_{s2}(r) = u_{s1}(r)\text{circle}(r)\text{pha}(r)$: Here $\text{circle}(r)$ is the amplitude modulation function, which equals 1 when $r < 12.7 \text{ mm}$ and equals 0 when $r > 12.7 \text{ mm}$, and $\text{pha}(r) = \exp(-ikr^2/2f_1)$ is the phase modulation function of a lens, with f_1 being the focal length of the collimating mirror and k the wave vector of the pump laser. By repeating this calculation we obtain the final light field emitted by the gas cell as shown in Fig. 2(b). Compared with Fig. 2(a), the intensity distribution in Fig. 2(b) has a very similar shape but no oscillations. On-axis comparisons are shown in Figs. 3(a) and 3(b), from which we can see that the finite and infinite aperture curves have similar envelopes, but oscillations appear when the aperture size is infinite.

The differences in the simulation results of Figs. 1 and 2 result from the fact that the size of the TB beam is much larger than the size of any optical element. For comparison, the Gaussian beam is assumed to have a waist of diameter 125 μm at the exit of the hollow fiber. After arriving at the front surface of the collimating mirror it has the profile (blue [gray] dashed line) shown in Fig. 4, where the red (gray) line is

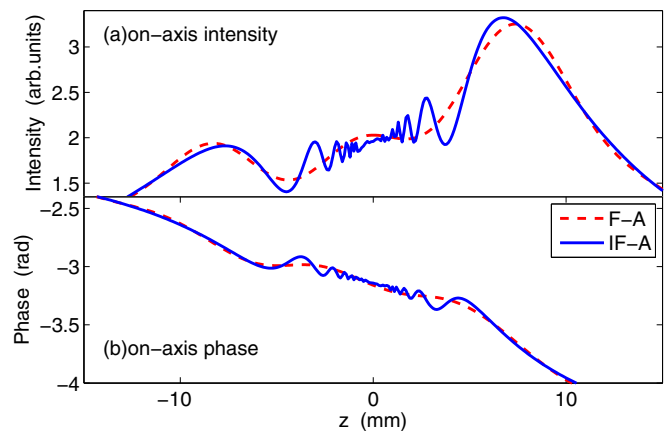


FIG. 3. (Color online) On-axis ($r = 0$) intensity (a) and phase (b) distributions of TB beam around the laser focus. Solid blue (gray) line: infinite-aperture (IF-A); red (gray) dashed line: finite-aperture (F-A).

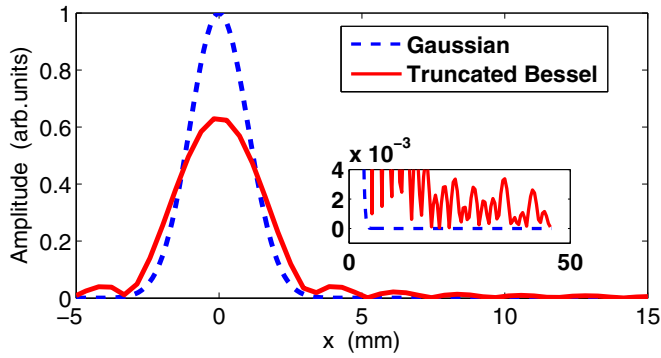


FIG. 4. (Color online) Amplitude profile of the TB beam (red [gray] line) and the Gaussian beam (blue [gray] dashed line) at the front surface of the collimating mirror. The inset is an enlargement of the outer edge of the TB beam.

the amplitude distribution of the TB beam. Both beams seem to have a diameter of less than 12 mm, well within the 25.4-mm diameter of the spherical mirror, which can thus be regarded as infinite in size. However, if we look at an enlargement of the wings of the profile, as shown in the inset, beyond $x > 20$ mm the Gaussian beam nearly vanishes but the TB beam still has an amplitude at the level of 10^{-3} . Previous authors assumed an infinite size for all the optical elements, so these weak amplitudes were included in their simulations, resulting in the fast oscillations of Figs. 2(a) and 3 (blue [gray] line). However, in real experiments all the optical elements have finite size, so those weak amplitudes located far outside the collimating mirror should be neglected. Our method takes the finite size into account and plots the actual light field, which does not exhibit any fast oscillations near the laser focus, as can be seen in Figs. 2(b) and 3 (red [gray] dashed line).

III. METHOD: FLATTENING THE PHASE FRONT CURVATURE OF HIGH-ORDER HARMONICS

The spatial distribution of the TB beam near the laser focus has been analyzed in the previous section. In this section we show how to utilize the TB beam to generate high-order harmonics with minimal angular divergence. In second-order harmonics (SOH) generation, the pump laser is focused into a nonlinear crystal. The crystal would emit an SOH laser beam with a photon energy twice that of the pump laser. Its phase $\phi_2(r, z)$ and that of the pump laser $\phi_1(r, z)$ are related by the equation $\phi_2(r, z) = 2\phi_1(r, z)$, so the spatial distribution of its phase is a direct copy of that of the pump. For a Gaussian pump laser the phase front around the waist is flat in the radial direction, so the SOH also has a flat phase front with a small angular divergence in the far field. In HHG the phase of the q th-order harmonic is the sum of the two terms in Eq. (1): Around the focus the phase front of the first term is flat but that of the second is not, so the total phase front is curved. Putting the gas jet exactly at the focus would lead to a large HHG divergence. Moreover, at this position the harmonics from short and long trajectories would overlap with each other [22] and interfere, resulting in bad spatial characteristics with messy modulations [7,23].

The phase of high-order harmonic comprises the laser phase and the intensity-dependent atomic-dipole phase. The two phase fronts bend in opposite directions so at a certain position the wavefront of the total phase may become flat. If c_q is half the curvature of the phase front of the q th order harmonic, it can be calculated by the equation

$$2c_q(r, z) = \frac{\phi_q''(r, z)}{[1 + \phi_q'^2(r, z)]^{\frac{3}{2}}}, \quad (2)$$

where $\phi_q'(r, z)$ and $\phi_q''(r, z)$ are the first-order and second-order derivatives of $\phi_q(r, z)$ with respect to r , respectively. For an axial-symmetric system the on-axis ($r = 0$) curvature can be simplified to $2c_q(z) = \phi_q''(z)|_{r=0}$, so c_q can be written as

$$c_q = qc_{\text{laser}} + c_{\text{int}}, \quad (3)$$

where c_{laser} and c_{int} are the half-curvatures of the laser phase front and intensity-dependent atomic dipole phase front, respectively. For a Gaussian beam, c_q can be expressed by the following equation [22]:

$$c_q = \frac{qk}{2R_z} - 2\alpha \frac{I_{0z}}{w_z^2}, \quad (4)$$

where R_z , w_z , and I_{0z} are the wavefront radius, beam size, and the on-axis ($r = 0$) intensity, respectively, at position z . The first term is negative when $z < 0$ and positive when $z > 0$, as can be seen from the dashed line in Fig. 5(a), which shows the curvature as a function of z . Since α is always negative, the total curvature $2c_q$ may be zero when the gas cell is put in front of the laser waist ($z < 0$). Actually, when it is placed at $z = -8$ mm, the total phase front is flat (as demonstrated in our previous work [22]). However, at this position, the light intensity drops dramatically to less than 50% of the peak intensity at $z = 0$. This low intensity would result in low efficiency and a waste of the light energy. For a low energy femtosecond laser (mJ level) it is not practical to generate high-order harmonics with the gas cell at this position.

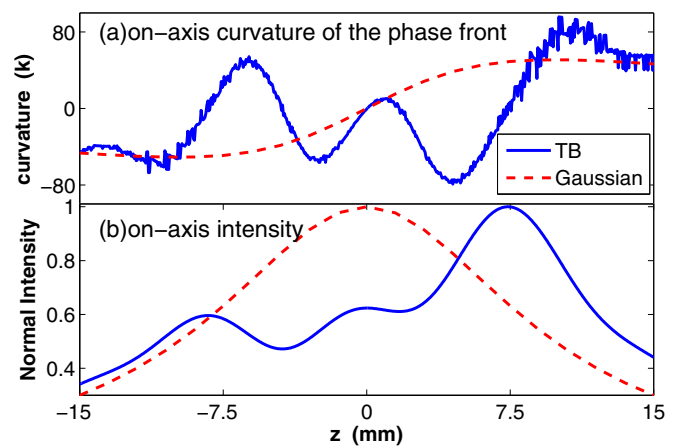


FIG. 5. (Color online) (a) On-axis ($r = 0$) curvature of the laser phase front. The vertical axis is in units of the absolute value of the pump laser wave vector k . (b) On-axis intensity. The laser beam has a $60\text{-}\mu\text{m}$ Gaussian waist. The TB beam is the same as that in Fig. 1(a). Solid line (blue [gray]): TB beam; dashed line (red [gray]): Gaussian beam; $z = 0$ is the position of the laser focus.

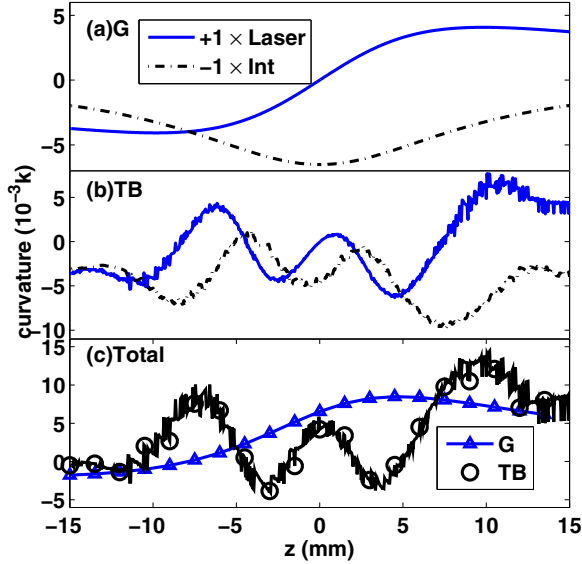


FIG. 6. (Color online) Panels (a) and (b) show the q times the laser phase curvature ($+1 \times \text{laser}$) (blue [gray] solid line) and the -1 times the intensity-dependent atomic-dipole phase curvature ($-1 \times \text{int}$) (black dot-dashed line) for Gaussian beam and TB beam respectively. Panel (c) shows the phase front curvatures of high-order harmonics for the Gaussian beam (blue [gray] triangle) and the TB beam (black circle). Laser intensity is $8 \times 10^{14} \text{ Wcm}^{-2}$. The harmonic order q is 80. Wavelength of pump laser is 800 nm. $\alpha = -4 \times 10^{-14} \text{ cm}^2 \text{ W}^{-1}$.

The TB beam has two on-axis intensity peaks at $z = -8.3 \text{ mm}$ and $z = 7.2 \text{ mm}$, as shown in Fig. 5(b) (solid line) and Fig. 2(b). Its curvature as a function of z is very different from that of the Gaussian beam, as can be seen from the solid line in Fig. 5(a). Around $z = 4 \text{ mm}$ its curvature reaches an extremum with an absolute value larger than that of the Gaussian beam. This large negative curvature can be used to cancel the large positive curvature of the atomic-dipole phase front. Moreover, at this position the light intensity only drops to 80% of the peak intensity, as can be seen from the solid line in Fig. 5(b). This TB beam can therefore simultaneously fulfill the two requirements of large negative curvature of the phase front and high light intensity, so it can be used to generate high-order harmonics with small angular divergence.

The curvatures of the two phase fronts of Eq. (3) are shown in Fig. 6. The results for the Gaussian beam are shown in Fig. 6(a). The solid line is the laser phase curvature, and the black dot-dashed line is the atomic-dipole phase curvature which we have drawn reversed to show the crossover of the two lines; at this crossing point the two curvatures of the two phase fronts have the same absolute values but exactly opposite signs, so the harmonic has a flat phase front. For the Gaussian beam, as discussed above, the position of cancellation is around $z = -8 \text{ mm}$, where the laser intensity is too low so it is unpractical experimentally. Figure 6(b) shows the results for the TB beam. Several crossings exist around the laser focus. We see, especially, that around $z = 5 \text{ mm}$, the laser intensity is strong enough for practical use. The total curvatures can be seen in Fig. 6(c). As expected, the zero curvature point for

the Gaussian beam is around $z = -8 \text{ mm}$. For the TB beam, a new feature appears: Around $z = 4 \text{ mm}$, the curvature of the harmonic phase front exhibits an extremum, so around this position it varies slowly. This is beneficial for phase matching. Another mechanism is mentioned by Altucci *et al.* [15]. In their paper, fast laser pump oscillations, which are not present in our model, are considered to cause stable points which are beneficial for phase matching. In our work, phase matching favors the emergence of extreme points, which can lead to a long phase matching area for the TB beam. For a Gaussian beam (blue [gray] triangles in Fig. 6 (c)), around $z = 4 \text{ mm}$ the curvature also reaches an extremum. The slow variation of the high-order harmonic phase front along the z direction can explain a well-known fact: The region several millimeters behind the laser focus of a Gaussian beam is good for phase matching. This explanation is in accordance with the phase matching map of Ref. [9], which takes into account the gradient of the harmonic phase.

IV. EXPERIMENT AND SIMULATION

In the experiment a 5-fs laser pulse with 0.4 mJ energy is used. The gas cell is a sealed nickel tube 1 mm in diameter filled with neon gas to a pressure of around 20 kPa. The laser pulse is focused such that it burns a hole through both sides of the tube wall, and thus creates a tunnel for the generated high-order harmonics to pass through. These harmonics are then focused by a toroidal mirror and diffracted by a flat-field grating into a soft x-ray charge-coupled device (CCD) camera, in which the far field spectrum is recorded.

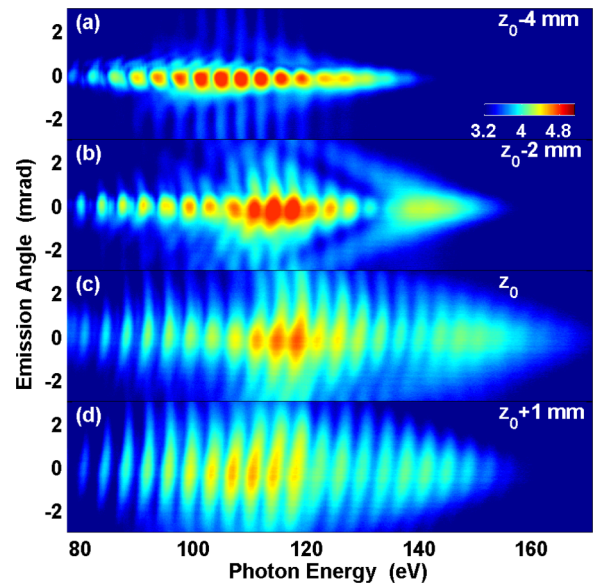


FIG. 7. (Color online) High-order harmonics spectra recorded in the far field. The highest order harmonics are produced in panel (c), where the laser intensity is around its peak value [$z = 7.2 \text{ mm}$ from the focus, as shown in Fig. 5(b)]; this position of the gas cell is defined as z_0 . Other distances of the cell are denoted in the upper right-hand corners. In panels (a), (b), and (d), the cell is located 4 and 2 mm in front of and 1 mm behind z_0 , respectively. All color bars are on the same log scale.

The high-order-harmonics spectra are shown in Fig. 7. The highest order harmonics are realized in Fig. 7(c), where the pump intensity is approximately at its maximum and corresponds to a cell position of about $z = 7.2$ mm from the focus (Fig. 3). This position is defined as z_0 in Fig. 7. When the cell is moved in the positive z direction, as shown in Fig. 7(d), the order and intensity of the harmonics decrease, while the divergence increases. When the cell is moved closer to the focus along the negative z direction, as shown in Figs. 7(b) and 7(a), the harmonic intensity increases but the divergence is reduced so the high-order harmonics form a bright beam of small angular divergence. The brightness of harmonics in Fig. 7(a) is much greater than that in Fig. 7(d). Figures 7(a) and 7(b) correspond to the region around the extremum $z = 4$ mm in Fig. 6(c). This result verifies our above analysis that three characteristics, namely, a relatively high pump intensity, a small harmonic phase curvature, and a slowly varying harmonic phase front around an extremum, are beneficial for the generation of bright high-order harmonics with small angular divergence. An important experimental condition which should be mentioned is that the carrier-envelope phase (CEP) of the pump laser was stabilized, so the harmonic spectra in Fig. 7 were obtained with the same CEP. The CEP-dependent harmonic spectrum was described in our previous work [24].

For comparison, numerical simulations were made. The single-atom response of HHG was calculated based on the strong-field approximation model [6]. The propagation of high-order harmonics was calculated based on the paraxial wave function [25,26]. In the model, laser-induced free-electron oscillation is the source of the propagation equation of the pump laser, and the calculated harmonic dipole moment is the source of the propagation equation of the harmonics. The parameters in our simulation were the same as those in the experiment except that the length of the gas cell was taken to be 0.1 mm and the focal length of the collimating mirror was 0.7 m. The results are shown in Fig. 8. Figure 8(c) shows the spectrum when the harmonics reach the highest order. When the gas cell is moved in the positive z direction as shown in Fig. 8(d), the intensity drops and the divergence increases. When moved in the negative z direction as shown in Figs. 8(b) and 8(a), the intensity is enhanced and the divergence decreases. These characteristics are in accordance with the experimental results shown in Fig. 7.

It should be explained why the cell length and focal length of the collimating mirror in the simulation were chosen to be different from the actual experimental values. The reason for the latter was to make the simulated beam size around the laser focus the same as that in the experiment. The selection of a shorter cell was for two reasons. First, the result would show that the conclusion of this paper is that the spatial distribution of the high-order harmonics depend mainly on the r and not the z distribution of the phase. Second, although the real cell was 1 mm in length, the actual interactive length may be far less than 1 mm, which was also discussed in previous studies [1,27]. The phase matching of the few-cycle TB laser beam with finite aperture size, including the extrema of the phase front curvature, will be discussed in detail in a following paper.

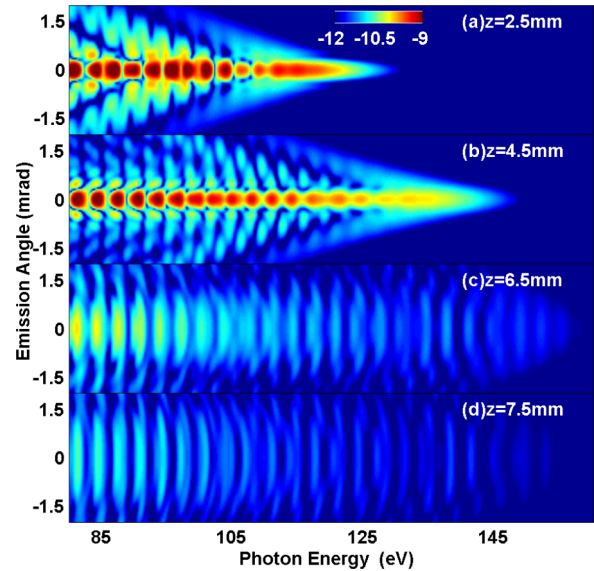


FIG. 8. (Color online) Simulated high-order-harmonic spectra in the far field for a laser intensity of $8 \times 10^{14} \text{ W cm}^{-2}$. From panels (a) to (d), the gas cell is moved along the positive z direction. The values of z correspond to the positions in Fig. 3. All color bars are on the same log scale.

V. DISCUSSION

For the benefit of practical experiments, we now describe when one should take the finite size of optical element into account for the maximum amount of laser energy to be enclosed by the optical elements.

A Gaussian beam is assumed to propagate freely from plane A to plane B. In both planes most of the energy ($>99.99999\%$) is concentrated within the ranges $r < r_a$ and $r < r_b$, where r_a and r_b are the radii of the optical elements in planes A and B, respectively. Any other beam with a greater energy inside $r < r_a$ in plane A may undergo stronger diffraction, so its energy may flow out of the range of $r < r_b$ in plane B. Thus the optical element in plane B may be regarded as infinite for a Gaussian beam but as finite for other beams. Even when all optical elements can be considered as being infinite in size for a Gaussian beam, whether we should take their finite size into consideration depends on the degree of the beam's spatial constraint. A beam is well constrained in a plane when its energy is concentrated at the center ($r = 0$) and no oscillations of the intensity exist in large r areas. The oscillation may lead to the flow of energy to large r areas. If a beam is well constrained both in the initial plane A and in plane B at infinity, it is well constrained in the whole propagation process and is spatially well constrained. The field distribution at plane B is the Fourier transform of the distribution at plane A, so in other words, if a beam is well constrained both in space and in the spatial-frequency domain at the initial plane, it is spatially well constrained. The Gaussian and TB beams are both well constrained at the output plane of a hollow fiber in space, while in the spatial frequency domain the former is well constrained but the latter is not and will diverge greatly.

In our case of Fig. 4 at the front surface of the collimating mirror, 99.999988% of the Gaussian beam energy is

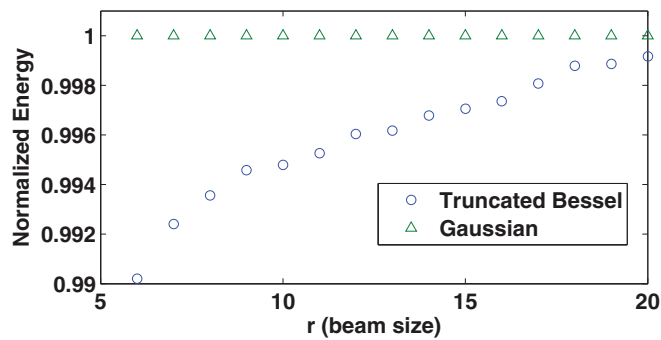


FIG. 9. (Color online) Convergence of the field energy as a function of r at the front surface of the collimating mirror of Fig. 1. The unit of radial direction is the beam size for both the TB and Gaussian beams. The y axis denotes the light energy inside the area of r .

concentrated within the range of $r < 3r_{0G}$, while only 97.9791190% of the TB beam energy lies in the area within $r < 3r_{0TB}$, where r_{0G} and r_{0TB} are the beam sizes of the Gaussian and the TB beams, respectively. The beam size is defined as the radius where the light intensity drops to e^{-2} of the peak intensity. The convergences of energy for both beams are shown in Fig. 9, where we can see that the Gaussian beam shows a fast convergence but for the TB beam more than 0.2% of the energy is still outside the area of $15r_{0TB}$. Therefore, the mirror of 25.4 mm diameter can be seen as infinite for a Gaussian beam but as finite for a TB beam. For a bad spatially constrained beam, such as the TB beam, we should look into the details of its field distribution at every optical element.

Finally, one important thing that must be mentioned is that the characteristics of the TB beam discussed in this paper and previous works result from its being truncated by the hollow fiber and not its Bessel spatial distribution. Any beam, such as a Gaussian beam, if truncated by a hard aperture would have

a similar spatial distribution as the TB beam around the laser focus point.

VI. CONCLUSION

In conclusion, in this paper we investigated the generation of high-order harmonics with minimized angular divergence driven by a truncated Bessel beam which propagates through optical elements of finite size. Mirrors with finite-size apertures further truncate the TB beam, so around the laser focus the spatial distribution of the TB beam is smooth and exhibits no fast oscillations but has two intensity peaks around the laser focus. Just in the front of the second peak the large curvature of the laser phase front cancels that of the intensity-dependent atomic-dipole phase front and leads to a flat phase front of the high-order harmonics. This characteristic combined with the relatively high pump intensity makes this a good position for generating bright high-order harmonics with small angular divergence. Moreover, for the high-order harmonics several extrema of the curvature of the phase front around the laser focus are beneficial for phase matching. This work has practical importance because hollow fibers are widely used in the field of ultrafast science. Our work, as a supplement to previous works [14–16], provides a new way to generate bright high-order harmonics with small angular divergence so that the total phase front of the harmonics becomes flat.

ACKNOWLEDGMENTS

The authors thank Ling-An Wu for revision of the manuscript. This work is partially supported by the National Basic Research Program of China (Grants No. 2013CB922401 and No. 2013CB922402), the National Major Instrument Program of China (Grant No. 2012YQ120047), the National Natural Science Foundation of China (Grants No. 11174361 and No. 61205130), and International Joint Research Program of National Natural Science Foundation of China (Grant No. 61210017).

-
- [1] A. Shiner, B. Schmidt, C. Trallero-Herrero, H. Wörner, S. Patchkovskii, P. Corkum, J. Kieffer, F. Légaré, and D. Villeneuve, *Nat. Phys.* **7**, 464 (2011).
 - [2] R. L. Sandberg, A. Paul, D. A. Raymondson, S. Hädrich, D. M. Gaudiosi, J. Holtzner, R. I. Tobey, O. Cohen, M. M. Murnane, H. C. Kapteyn, C. Song, J. Miao, Y. Liu, and F. Salmassi, *Phys. Rev. Lett.* **99**, 098103 (2007).
 - [3] X. He, M. Miranda, J. Schwenke, O. Guilbaud, T. Ruchon, C. Heyl, E. Georgadiou, R. Rakowski, A. Persson, M. B. Gaarde, and A. L’Huillier, *Phys. Rev. A* **79**, 063829 (2009).
 - [4] Gy. Farkas and Cs. Tóth, *Phys. Lett. A* **168**, 447 (1992).
 - [5] P. B. Corkum, *Phys. Rev. Lett.* **71**, 1994 (1993).
 - [6] M. Lewenstein, P. Balcou, M. Y. Ivanov, A. L’Huillier, and P. B. Corkum, *Phys. Rev. A* **49**, 2117 (1994).
 - [7] P. Salières, A. L’Huillier, and M. Lewenstein, *Phys. Rev. Lett.* **74**, 3776 (1995).
 - [8] P. Salières, T. Ditmire, M. D. Perry, A. L’Huillier, and M. Lewenstein, *J. Phys. B—At. Mol. Opt.* **29**, 4771 (1996).
 - [9] P. Balcou, P. Salières, A. L’Huillier, and M. Lewenstein, *Phys. Rev. A* **55**, 3204 (1997).
 - [10] M. Lewenstein, P. Salières, and A. L’Huillier, *Phys. Rev. A* **52**, 4747 (1995).
 - [11] V. V. Strelkov, E. Mvel, and E. Constant, *New J. Phys.* **10**, 083040 (2008).
 - [12] W. Boutu, T. Auguste, O. Boyko, I. Sola, P. Balcou, L. Binazon, O. Gobert, H. Merdji, C. Valentin, E. Constant, E. Mével, and B. Carré, *Phys. Rev. A* **84**, 063406 (2011).
 - [13] P. Rudawski, C. M. Heyl, F. Brizuela, J. Schwenke, A. Persson, E. Mansten, R. Rakowski, L. Rading, F. Campi, B. Kim, P. Johnsson, and A. L’Huillier, *Rev. Sci. Instrum.* **84**, 073103 (2013).

- [14] M. Nisoli, E. Priori, G. Sansone, S. Stagira, G. Cerullo, S. De Silvestri, C. Altucci, R. Bruzzese, C. de Lisio, P. Villoresi, L. Poletto, M. Pascolini, and G. Tondello, *Phys. Rev. Lett.* **88**, 033902 (2002).
- [15] C. Altucci, R. Bruzzese, C. de Lisio, M. Nisoli, E. Priori, S. Stagira, M. Pascolini, L. Poletto, P. Villoresi, V. Tosa, and K. Midorikawa, *Phys. Rev. A* **68**, 033806 (2003).
- [16] C. Jin and C. D. Lin, *Phys. Rev. A* **85**, 033423 (2012).
- [17] W. Zhang, H. Teng, C.-X. Yun, P. Ye, M.-J. Zhan, S.-Y. Zhong, X.-K. He, L.-F. Wang, and Z.-Y. Wei, *Chin. Phys. Lett.* **31**, 084204 (2014).
- [18] W. Zhang, H. Teng, C.-X. Yun, X. Zhong, X. Hou, and Z.-Y. Wei, *Chin. Phys. Lett.* **27**, 054211 (2010).
- [19] A. E. Siegman, *Lasers* (University Science Books, Mill Valley, CA, 1986), p. 661.
- [20] J. S. A. Collins, *J. Opt. Soc. Am.* **60**, 1168 (1970).
- [21] J. Goodman, *Introduction to Fourier Optics* (McGraw-Hill, New York, 2008).
- [22] P. Ye, X.-K. He, H. Teng, M.-J. Zhan, S.-Y. Zhong, W. Zhang, L.-F. Wang, and Z.-Y. Wei, *Phys. Rev. Lett.* **113**, 073601 (2014).
- [23] J. Peatross and D. D. Meyerhofer, *Phys. Rev. A* **51**, R906 (1995).
- [24] P. Ye, X.-K. He, H. Teng, M.-J. Zhan, W. Zhang, L.-F. Wang, S.-Y. Zhong, and Z.-Y. Wei, *J. Opt. Soc. Am. B* **31**, 1355 (2014).
- [25] E. Priori, G. Cerullo, M. Nisoli, S. Stagira, S. De Silvestri, P. Villoresi, L. Poletto, P. Ceccherini, C. Altucci, R. Bruzzese, and C. de Lisio, *Phys. Rev. A* **61**, 063801 (2000).
- [26] Z. Chang, *Fundamentals of Attosecond Optics* (CRC Press, Boca Raton, FL, 2011).
- [27] C. Haworth, L. Chipperfield, J. Robinson, P. Knight, J. Marangos, and J. Tisch, *Nat. Phys.* **3**, 52 (2006).